APPLIED PHYSICS

Trapped particle makes 3D images

A technique in which a small particle is trapped and moved by laser light has been used to produce visual representations of objects in three dimensions, offering key advantages over currently used approaches. SEE LETTER P.486

BARRY G. BLUNDELL

Devices known as volumetric displays allow 3D images to be generated in a transparent enclosure. Because these images occupy three dimensions, they exhibit the spatial characteristics that we associate with real-world scenes. The images can be viewed without the need for glasses by many simultaneous observers, and changes in vantage point allow content to be seen from different orientations. On page 486, Smalley *et al.*[1] describe an innovative approach to volumetric-display implementation that allows 3D images to be formed in the air, removing the need for a transparent enclosure.

For more than 100 years, volumetric displays have been the subject of extensive research[2]. Although it is relatively easy to make a small (tabletop) display that works fairly well, it is extremely difficult to develop a larger display that works very well. There are two overarching (but often conflicting) problems. The first relates to the techniques that are currently used to produce dynamic images of relatively high visual quality. The second concerns the optical characteristics of the imaging volume, which must allow light emanating from the image to propagate, and emerge from the volume, without distortion — think of the distortion that occurs when light emerges from a tropical-fish tank.

With respect to the first problem, in most volumetric displays, the imaging volume is formed by the cyclic motion of a transparent surface (Fig. 1a). To produce a 3D image, a sequence of image slices is depicted on the surface as it moves through the volume. Given the need to refresh images at least 30 times per second to avoid perceptible flicker[3], the surface must move rapidly.

The motion of the surface can be either translational (along a straight line) or rotational. When translational motion is used, the dimensions of the imaging volume are limited by mechanical issues arising from the surface's mass and acceleration. In the case of rotational motion, the surface's linear speed increases with distance from the axis of rotation. This impinges on image quality and so can ultimately restrict the diameter of the imaging volume. There is also a 'dead' region in the vicinity of the rotational axis, in which image points cannot be formed[4].

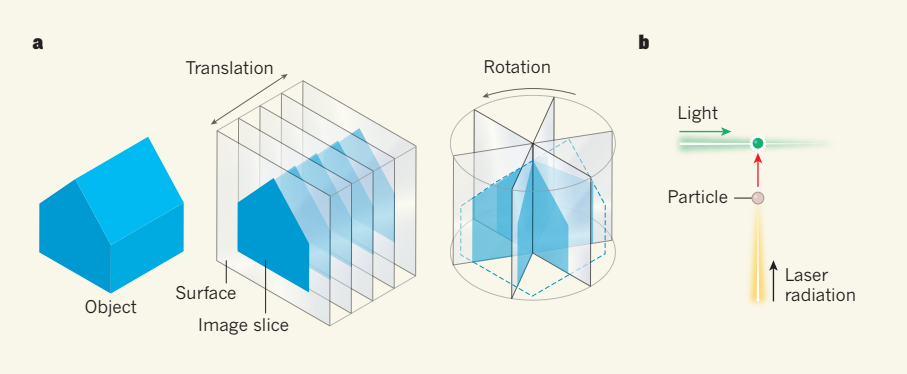

Figure 1 | Volumetric-display techniques. **a**, Devices known as volumetric displays can produce visual representations of objects in three dimensions. They typically use the rapid, cyclic motion of a transparent surface. To generate a 3D image, a sequence of image slices is depicted on the surface as it moves. This motion can be either translational (along a straight line) or rotational. **b**, Smalley *et al.*[1] report an alternative approach in which non-visible laser radiation is used to move a small particle (red arrow). To create an image point, the particle is illuminated with light as it passes through the required position.

A further limitation of these displays is that the surface's movement precludes the insertion of haptic probes — tools that recreate the sense of touch by applying forces, motion or vibrations to the user. Such probes can simulate the solidity associated with physical versions of images, so that, for example, virtual clay could be moulded and would feel like real clay.

Smalley *et al.* sought to overcome all of these difficulties using the photophoretic effect[5], whereby laser light is used to trap and move small particles (with diameters of 5–100 micrometres). To create a point of light at a given location in 3D space, the authors used non-visible laser radiation to move a particle, and as the particle passed through the required position, it was illuminated with red, green or blue light (Fig. 1b). The authors suggest that complex, high-fidelity, dynamic images could be formed by introducing parallelism — the simultaneous movement of many particles.

There are at least three key advantages of Smalley and colleagues' approach. First, it does not require the cyclic motion of a surface — movement is restricted to that of low-mass particles. Second, the presence of these particles will have minimal impact on the propagation of light through the imaging volume. And third, because the image is formed in the air, image components can coexist with haptic probes and other interaction tools.

The authors provide several photographs of image content produced using their technique (see Figure 2 of the paper[1]). However, these photographs required long exposure times — of the order of tens of seconds. For implementing a viable display, there is therefore a pressing need to explore ways of increasing the speed of particle motion and of introducing parallelism such that many image points can be created simultaneously.

The introduction of a high degree of parallelism poses a further challenge, relating to the fact that each point in the imaging volume must be individually accessible. This is reminiscent of an equivalent problem that was encountered in the late 1960s, in connection with a type of 3D display called a photochromic-based volumetric display[6,7]. Another concern is that the insertion of haptic probes into the image volume will probably give rise to shadow regions that will interfere with the propagation of light used for particle motion and illumination. However, the judicious design of such probes would ameliorate this potential problem.

In terms of photorealism, it is unlikely that these devices will ever directly compete with high-end stereoscopic 3D displays. However, despite more than a century of research into volumetric displays, there has been relatively

little work on exploring ways of capitalizing on key image characteristics. In particular, volumetric displays provide considerable freedom in viewing position, and support both vertical and horizontal motion parallax, which means that observers can move and change their view of an image in a wholly natural way.

Consequently, these devices offer exciting, and largely unexplored, opportunities to advance spatial imaging (in areas such as neurosurgery) and dynamic imaging (in fields including fluid dynamics, robotics and sports training). With regard to the latter, there is a need to better support the visualization of complex forms of 3D motion[8]. Moreover, creating volumetric images in the air enables direct interaction, thereby allowing, for example, 3D design tasks to be carried out in a natural way in 3D space.

Smalley and colleagues' approach could provide the foundation for the next generation of volumetric displays. Such devices will not only enhance our understanding of complex spatial and geometric dynamics, but also support innovative user interaction. ■

Barry G. Blundell *is with the University of Derby Online Learning (UDOL), University of Derby, Derby DE22 1GB, UK.*
e-mail: barry.blundell@physics.org

1. Smalley, D. E. *et al. Nature* **553,** 486–490 (2018).
2. Luzy, E. & Dupuis, C. Procédé pour obtenir des projections en relief. French Patent 461,600 (1914).
3. Blundell, B. G. *Enhanced Visualization: Making Space for 3-D Images* 68 (Wiley, 2007).
4. Blundell, B. G. & Schwarz, A. *Volumetric Three-Dimensional Display Systems* 72–91 (Wiley, 2000).
5. Davis, E. J. *Aerosol Sci. Technol.* **26,** 212–254 (1997).
6. Adamson, A. W. Method and apparatus for generating three-dimensional patterns. US Patent 3,609,706 (1971).
7. Adelman, A. H. & Lewis, J. D. Method and apparatus for generating three-dimensional patterns. US Patent 3,609,707 (1971).
8. Blundell, B. G. *3D Res.* **8,** 11 (2017).

STRUCTURAL BIOLOGY

Ageing-related receptors resolved

Ageing is a regulated process in which hormones have pivotal roles. Crystal structures of two hormone co-receptors should be informative for drug discovery focused on age-related disorders. SEE ARTICLE P.461 & LETTER P.501

MAKOTO KURO-O

In Greek mythology, three goddesses known as the Fates govern the lifespan of each person. Klotho, Lachesis and Atropos are the spinner, the allotter and the cutter of the thread of life, respectively. So when a genetic mutation was identified in mice that undergo premature ageing[1], the gene involved was fittingly named *klotho*. The protein it encodes, α-klotho, and a sister protein called β-klotho, are high-affinity co-receptors for certain members of the fibroblast growth factor (FGF) family of signalling proteins[2], but their means of action has not been well characterized. Two papers[3,4] in this issue describe crystal structures of FGF–klotho complexes, not only providing a basis for understanding how klothos act, but also opening up avenues for structure-based drug design.

α-Klotho is a membrane-spanning protein expressed predominantly in the kidney, as well as in the brain. Mice lacking α-klotho exhibit a range of signs associated with ageing, including hearing loss, impaired cognition and organ atrophy[5]. They also have elevated blood phosphate levels. However, the protein's function on the molecular level was unclear, until mice lacking FGF23 were characterized[6].

FGF23 is one of the three endocrine FGFs, which act as hormones, secreted by one organ to regulate the function of another. Specifically, FGF23 is secreted from bones after phosphate intake and acts in the kidney to inhibit phosphate reabsorption in urine, thereby maintaining the body's phosphate balance. Mice lacking FGF23 have elevated phosphate levels owing to impaired phosphate excretion, and exhibit features associated with ageing[6]. This striking similarity to mice lacking α-klotho led researchers to discover[2] that α-klotho forms a complex with the membrane-spanning protein FGF receptor 1c (FGFR1c), acting as a co-receptor to recruit FGF23 and so triggering FGF signalling

In the first of the current studies, Chen *et al.*[3] (page 461) solved the crystal structure of FGF23 in complex with the ligand-binding domain of FGFR1c and the extracellular domain of α-klotho. The structure revealed that α-klotho (aptly, given its namesake) sends out a long receptor-binding arm (RBA) that acts as a thread to capture the ligand-binding domain of FGFR1c. Indeed, when the authors generated α-klotho lacking the RBA, the mutant protein failed to capture FGFR1c or to help FGF23 to activate FGF signalling.

Chen and colleagues showed that FGF23 fits into the groove created between α-klotho and FGFR1c. The globular amino-terminal region and the rod-like carboxy-terminal region of FGF23 face FGFR1c and α-klotho, respectively (Fig. 1). By promoting formation of this complex, α-klotho enables strong interactions between FGF23 and FGFR1c, which otherwise interact only weakly.

Like α-klotho, β-klotho functions as a co-receptor for endocrine FGFs, forming a complex with FGFR1c to bind FGF21, and with FGFR4 to bind FGF19 (refs 7,8). FGF19 is secreted from the intestine after feeding, and acts in the liver to suppress bile-acid synthesis. FGF21 is secreted from the liver following fasting, and acts in fat cells and the brain to induce metabolic adaptation to fasting and responses to stress[5]. Although FGFRs are expressed in a wide range of tissues, the tissue-specific expression of β-klotho in the liver, fat and brain restricts the target organs of these endocrine FGFs.

In the second study, Lee *et al.*[4] (page 501)

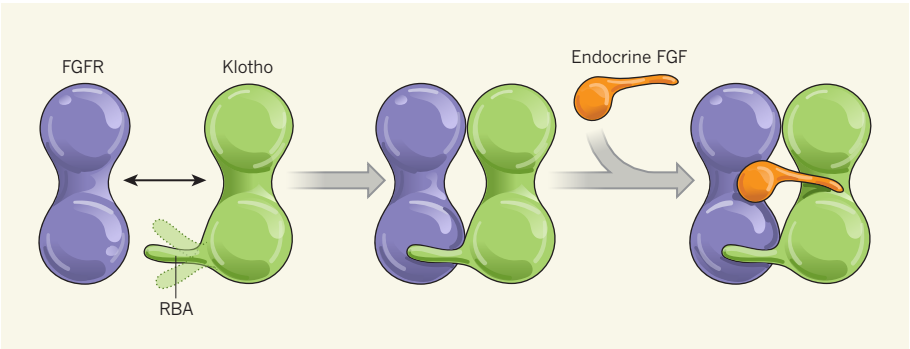

Figure 1 | Structures reveal the mode of action for klotho proteins. Two groups[3,4] have produced crystal structures of the extracellular domains of klotho proteins, either alone, in complex with 'endocrine' fibroblast growth factors (FGFs), or in complex with both endocrine FGFs and the ligand-binding domains of FGF receptors (FGFRs). As this simplified schematic shows, the klotho proteins seem to have an intrinsically disordered receptor-binding arm (RBA) with which they capture FGFRs (interaction indicated by double-headed arrow). The RBA enables formation of a stable complex, with FGFs fitting into the groove between the other two proteins.

resolved the crystal structure of β-klotho's extracellular domain when bound to and when free from FGF21, in the absence of FGFRs. Like FGF23, the C-terminal region of FGF21 fits into the groove in β-klotho. However, the authors could not solve the structure of some regions in β-klotho, including that corresponding to the RBA in α-klotho. This suggests that the RBAs of klotho proteins are intrinsically disordered and unable to fold stably unless bound to FGFRs. The fact that intrinsically disordered proteins can interact with multiple proteins[9] implies that the RBAs of klotho proteins could capture other partners besides FGFRs. This might explain why the extracellular domain of α-klotho, which can be released into the extracellular space, has been reported to have FGF-independent activity, regulating several ion channels and transporters, along with other growth factors and their receptors[5].

Another proposed FGF-independent activity for the klothos is as carbohydrate-binding proteins called lectins. Klothos belong to a family of enzymes that cut sugar chains[1], but not all of the amino-acid residues essential for this enzymatic activity are found in the klothos. Thus, klothos might bind to, but not cut, specific carbohydrates. Lee and colleagues' structure of β-klotho leaves open the possibility that this protein interacts with particular sugar chains. By contrast, Chen and co-workers' structure of FGF23–α-klotho–FGFR does not fit with the idea of α-klotho acting as either an enzyme or a lectin. However, it might be that in the absence of FGFRs, the structure of α-klotho would provide a different point of view. Alternatively, it is possible that the two klothos have different FGF-independent activities.

FGF–klotho signalling has key roles in ageing and age-related disorders. The new structures could be used to develop drugs to treat disorders of ageing, using structure-based drug design to identify targets in FGF–klotho–FGFR complexes. For instance, consider chronic kidney disease (CKD)[5,10] — a common state of impaired renal function that often occurs as a complication of high blood pressure or diabetes. People with CKD exhibit many of the same symptoms as mice lacking α-klotho, including disturbed phosphate metabolism and increased risk of death[5,10]. Placing mice lacking FGF23 or α-klotho on a low-phosphate diet reduces the phosphate retention and premature ageing normally seen in these animals, indicating that phosphate increases accelerate ageing[10]. Thus, drugs that target FGF–klotho–FGFR complexes to improve phosphate metabolism might be useful to treat CKD.

A second example lies in the targeting of FGF21 complexes. FGF21 overexpression extends lifespan in mice[11], and this protein has been dubbed an 'anti-ageing' hormone. Lee *et al.* demonstrated that they could increase the potency of FGF21 by introducing genetic mutations designed to increase the protein's affinity for β-klotho. Further analyses such as this could provide a way to explore anti-ageing medicines more generally. ■

Makoto Kuro-o *is in the Division of Anti-Ageing Medicine, Center for Molecular Medicine, Jichi Medical University, Shimotsuke, Tochigi 329-0498, Japan.*
e-mail: mkuroo@jichi.ac.jp

1. Kuro-o, M. *et al. Nature* **390,** 45–51 (1997).
2. Kurosu, H. *et al. J. Biol. Chem.* **281,** 6120–6123 (2006).
3. Chen, G. *et al. Nature* **553,** 461–466 (2018).
4. Lee, S. *et al. Nature* **553,** 501–505 (2018).
5. Hu, M. C., Shiizake, K., Kuro-o, M. & Moe, O. W. *Annu. Rev. Physiol.* **75,** 503–533 (2013).
6. Shimada, T. *et al. J. Clin. Invest.* **113,** 561–568 (2004).
7. Ogawa, Y. *et al. Proc. Natl Acad. Sci. USA* **104,** 7432–7437 (2007).
8. Kurosu, H. *et al. J. Biol. Chem.* **282,** 26687–26695 (2007).
9. Wright, P. E. & Dyson, H. J. *J. Mol. Biol.* **293,** 321–331 (1999).
10. Kuro-o, M. *Nature Rev. Nephrol.* **9,** 650–660 (2013).
11. Zhang, Y. *et al. eLife* **1,** e00065 (2012).

This article was published online on 17 January 2018.

ASTRONOMY

A beacon at the dawn of the Universe

Quasars are the brightest continuously emitting sources of radiation in the Universe. Measurements of the most distant quasar ever detected reveal details about the evolution and structure of the early Universe. **SEE LETTER P.473**

EILAT GLIKMAN

Since their discovery[1] in 1963, astronomical objects called quasars have been among our most powerful probes of the early Universe. Initially seen as mysterious sources of extreme luminosity, quasars are now known to be supermassive black holes that are voraciously consuming gas from their immediate surroundings, emitting large amounts of radiation in the process. On page 473, Bañados *et al.*[2] report observations of the most distant quasar found so far. The light detected from this object was emitted when the Universe was a mere 690 million years old — just 5% of its current age.

Almost 90 years ago, the astronomer Edwin Hubble discovered that the Universe is expanding[3]. The expansion stretches light waves travelling through space, such that light that was emitted from a distant source as blue might be detected as red. This phenomenon is called redshift, and is associated with both distance and time: the larger the redshift, the farther away the source was when it emitted its light, meaning that the light was emitted at an earlier time.

If we rewind the expansion, we find that the

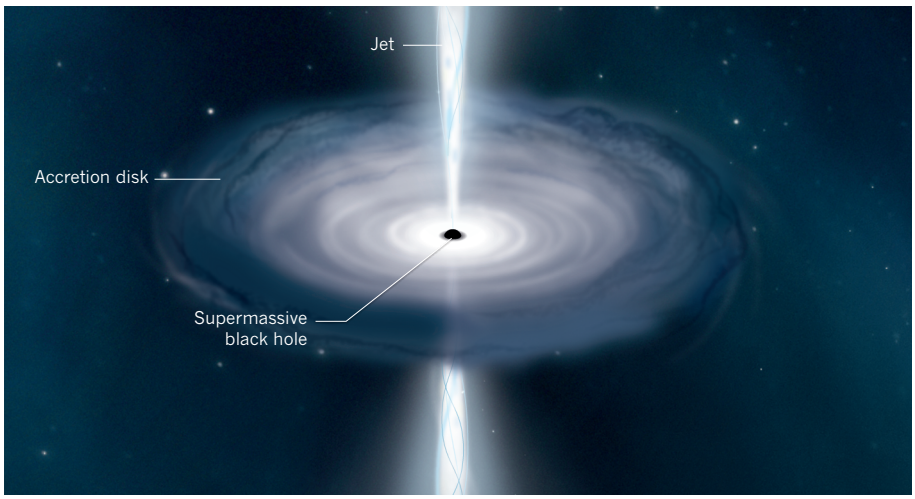

Figure 1 | Emission from a quasar. Quasars are extremely luminous astronomical objects that comprise a supermassive black hole surrounded by an orbiting disk of gas called an accretion disk. As material in the disk is pulled towards the black hole, energy is released in the form of electromagnetic radiation and, in some cases, as beams of charged particles called jets. Bañados *et al.*[2] report observations of the most distant quasar identified so far, the light of which was emitted when the Universe was only 5% of its current age.

Universe started out in a hot, dense state, filled mostly with ionized hydrogen. As it expanded, it also cooled, and after about 380,000 years, the temperature was low enough for neutral hydrogen to form. For the first few hundred million years, the Universe was devoid of any sources of light — no stars, galaxies or quasars existed. The first stars were then born, but the Universe remained dark because neutral hydrogen is highly effective at absorbing ultraviolet radiation (the main type of emission from these stars).

However, the present-day Universe is filled with sources of light, and the hydrogen that exists in the space between galaxies (the intergalactic medium) is completely ionized and therefore transparent to the ultraviolet emission from early galaxies and quasars. The process of this phase change from a neutral to an ionized Universe, known as reionization, is poorly understood.

The neutral fraction of hydrogen in the Universe can be estimated by analysing the absorption of light by hydrogen in quasars. Studies of quasars observed as they were when the Universe was 0.85 billion to 1.2 billion years old (corresponding to redshifts of 6.5 to about 5, respectively) have shown that the neutral fraction decreased sharply from 0.1% to 0.01% during this time[4]. However, most of the reionization process occurred before this epoch.

Bañados and colleagues' quasar, known as ULAS J1342+0928, has a redshift of 7.54. This means that its strong ultraviolet emission has been shifted into the near-infrared, beyond the sensitivity of typical imaging surveys of the sky. Finding such a high-redshift quasar was not possible until about a decade ago, when sufficiently sensitive near-infrared detectors began scanning large areas of the sky[5,6]. By studying the absorption spectrum of ULAS J1342+0928 (the fraction of incident radiation absorbed by the intergalactic medium over a range of frequencies), the authors determined that the neutral proportion of hydrogen was at least 10% when the Universe was 690 million years old, which sets a strong constraint on how the intergalactic medium was reionized.

The quasar's black hole is extremely massive — about 800 million times the mass of the Sun. Black holes grow by consuming (accreting) gas from a surrounding structure called an accretion disk (Fig. 1). The gas emits radiation as it falls in. However, such systems have a maximum luminosity, which occurs when the pressure of the emitted light pushes away the infalling gas, halting further growth. This luminosity depends on the mass of the accreting black hole, and therefore defines a maximum growth rate, known as the Eddington limit, for the system.

Bañados *et al.* suggest that the large mass of the black hole in ULAS J1342+0928 can be explained if the object began its life as an initial (seed) black hole of at least 1,000 solar masses. This result could rule out models in which black-hole seeds were created from the deaths of the first massive stars[7], and instead favour models in which these seeds formed from the direct collapse of primordial gas[8]. In addition, the black hole would need to have grown continuously (and, therefore, exponentially) at the Eddington limit, starting from when the Universe was roughly 65 million years old. Although this scenario is physically possible, it requires extreme, sustained accretion for about 600 million years, which is substantially longer than the typical lifetime of a quasar[9].

So far, only two quasars with redshifts greater than 7 have been discovered. The previous record holder was reported[10] in 2011, and early models of quasar evolution predicted that more should have been found by now[11]. The methods for finding quasars, even at these high redshifts, are sound and have been proved effective. Therefore, the dearth of high-redshift quasars might indicate that these objects were uncommon in the early Universe, and could imply a sharp decline in quasar activity towards early times[12]. If so, this suggests that we might be observing extremely rare systems as they were beginning to emerge in the Universe.

The authors' work offers a glimpse into the conditions of the intergalactic medium at the earliest epoch of structure formation in the Universe, and could place key constraints on cosmological models of this era. However, a single quasar is insufficient for providing a complete picture of the Universe in the reionization era or of the evolution and growth of supermassive black holes from initial seeds. The task ahead is, then, to mine the upcoming near-infrared sky surveys for additional quasars that can paint a more complete picture of the rapidly evolving early Universe. ■

Eilat Glikman *is in the Department of Physics, Middlebury College, Middlebury, Vermont 05753, USA.*
e-mail: eglikman@middlebury.edu

1. Schmidt, M. *Nature* **197,** 1040 (1963).
2. Bañados, E. *et al. Nature* **553,** 473–476 (2018).
3. Hubble, E. *Proc. Natl Acad. Sci. USA* **15,** 168–173 (1929).
4. Fan, X., Carilli, C. L. & Keating, B. *Annu. Rev. Astron. Astrophys.* **44,** 415–462 (2006).
5. Wright, E. L. *et al. Astron. J.* **140,** 1868–1881 (2010).
6. Lawrence, A. *et al. Mon. Not. R. Astron. Soc.* **379,** 1599–1617 (2007).
7. Natarajan, P. & Volonteri, M. *Mon. Not. R. Astron. Soc.* **422,** 2051–2057 (2012).
8. Bromm, V. & Loeb, A. *Astrophys. J.* **596,** 34–46 (2003).
9. Hopkins, P. F. & Hernquist, L. *Astrophys. J.* **698,** 1550–1569 (2009).
10. Mortlock, D. J. *et al. Nature* **474,** 616–619 (2011).
11. Fan, X. *et al. Astrophys. J.* **121,** 54–65 (2001).
12. McGreer, I. D. *et al. Astrophys. J.* **768,** 105 (2013).

SUSTAINABILITY

Satellite images show China going green

Large-scale tree-planting projects have taken place in regions of China prone to soil erosion. Satellite imagery reveals the effects of this work, and shows that a predicted vegetation decline didn't occur during a period of drought.

MARC MACIAS-FAURIA

The effects of human activities on Earth's vegetation have tended to be negative, mostly because of deforestation[1]. Restoration efforts are often restricted to small, localized scales. Large ecological-engineering projects aimed at producing regional-scale effects are few, and among these, China's mega-projects — most notably, the Grain for Green Project (GGP)[2] — stand out because of their unparalleled scale (27.8 million hectares of forest re-established as of 2013 across 26 Chinese provinces[3]). Writing in *Nature Sustainability*, Tong *et al.*[4] report that the positive effects of these tree-planting projects on vegetation growth can be detected using remote-sensing satellite imagery of a large region of southwestern China (the provinces of Guizhou, Guangxi and Yunnan), in an area associated with highly erodible landscapes called karst. The authors note that these projects, which require considerable investment, will be justified only if the modification of ecosystem properties can be achieved on a large scale.

The government-run GGP, intended to halt soil erosion and desertification, began in 1999 (ref. 2). The project's goal was to convert land on mountainous terrain prone to erosion (cropland or scrubland) into forested landscapes (Fig. 1). Such forest would be classified as ecological if trees might eventually be logged (subject to permission) as part of a timber quota, and as economical if it contained orchards, or plantations of trees for medical use. Ecological forest accounted for 80% of the planting area, with economical forest making up the remaining 20% (ref. 4). The GGP was developed partly in response to

Figure 1 | Trees planted as part of an ecological-engineering project in China. Tong *et al.*[4] report an analysis of the effects of a large-scale tree-planting project, called the Grain for Green Project, on mountainous regions of southwestern China that are associated with high levels of soil erosion. Shown here are some trees planted as part of this project in the Wolong Nature Reserve in the southwestern Sichuan province.

the consequences of land-use changes during the time of Chairman Mao Zedong, notably the huge areas logged to provide fuel and construction materials during the Great Leap Forward programme, and large-scale conversions of often marginal, sloping land to agricultural use in the 1960s and 1970s to enhance local self-sufficiency — a change that caused severe erosion problems[5].

To assess the effects of the tree-planting projects, Tong and colleagues use three independent lines of evidence, and the consistency of the findings convincingly demonstrate the robustness of their results. One approach was the analysis of two complementary properties of vegetation. Satellite-imaging data from 1982 to 2015 allowed the researchers to measure the area of vegetation cover present per square metre of ground (known as the leaf-area index). Other satellite data collected between 1992 and 2012 enabled the authors to assess plant biomass in units of above-ground carbon biomass. Plant biomass can be inferred by converting vegetation optical depth (a property captured by microwave observations that are sensitive to the water content of vegetation) to total carbon using an approach based on the carbon density of above-ground, living, woody vegetation.

Over time, both of these properties revealed a marked transition in the amplitude and/or direction of vegetation trends around the main implementation period of the tree-planting project, between 2000 and 2006. The authors' calculations indicate that the southwestern region of China that they studied acted as a carbon sink after the GGP implementation, providing a considerable amount of the entire country's net carbon sequestration. The authors also observed negative vegetation trends in the provinces' growing urban areas, such as in the cities of Kunming and Nanning. This provides an indirect validation of the team's satellite-data approach.

The second line of investigation taken by Tong *et al.* involved the use of dynamic ecosystem modelling to explore what might have happened in the absence of the tree-planting project. The model took into account the effect of the increase in atmospheric carbon dioxide on vegetation during the time frame studied. This modelling exercise highlighted the divergence between the simulated trend of vegetation decrease projected if the tree-planting intervention had not occurred — linked to a long-lasting drought during the previous decade — and the vegetation increase that was observed.

The third approach taken by the researchers was an analysis of the number of hectares on which tree-planting actions were implemented in each of the 295 counties within the 3 provinces studied. These GGP-inventory data showed a correspondence between actions at the county level and positive vegetation trends, as well as stark differences between China's provinces and the neighbouring countries of Laos, Vietnam and Myanmar, in which the vegetation assessed by satellite imagery decreased over the same period.

Tong and colleagues' results are encouraging in regard to the large-scale effects of the GGP on vegetation, but should not be taken as a proof of its overall success. As the authors mention, the satellite trends were not validated by measurements taken on the ground. No erosion assessment was undertaken, so one of the main GGP goals was not evaluated directly. Furthermore, the time span of satellite analysis, and of the programme itself, might still preclude the detection of long-term dynamics related to the long lifespan of trees, or might not take into account the role of large but infrequent erosion or disturbance events such as those linked to torrential rains or pest outbreaks.

Most crucial for the overall assessment of the success of the GGP as an ecological restoration project is the fact that satellite data do not distinguish biological composition, such as the presence of different species, and so cannot be used to assess the project's effects on biodiversity. The GGP focused on the planting of non-native, fast-growing monocultures, which might render the resulting forests more vulnerable to pests[3,4]. The GGP thus used a narrow view of ecosystem services (the role of vegetation in reducing erosion and desertification rates) that had the additional (and possibly unplanned) benefit of a net carbon-storage outcome. Furthermore, the rationale for GGP actions was based not on previous ecological states or projected overall ecological benefits, but on the potential to reduce the erosion rates on the target land and for the programme to generate income for farmers[2].

In the absence of a China-wide assessment of the GGP's environmental and ecological impacts[2], an analysis of data from China based on 258 publications[3] identified limited biodiversity benefits of the GGP. This was mainly because the dominant non-native, fast-growing monoculture plantations were linked to a decrease in floral diversity, associated with bee and bird population declines, as observed in Sichuan province. This report[3] strongly recommends using native trees when establishing plantations, or at least the establishment of plantations composed of several tree species.

Nevertheless, Tong and colleagues' work clearly shows a large-scale effect of the GGP on vegetation in southwestern China. This important result needs to be complemented by ground-based studies. Understanding of the GGP's functional and biodiversity effects is needed to assess its success, and might also identify other interventions that have the potential to enhance or generate wider positive effects of the GGP as an ecological-restoration mega-project. The task set out by Tong and colleagues for how the effects of such massive initiatives can be tested on an adequate scale is valuable and very welcome. ■

Marc Macias-Fauria *is at the School of Geography and the Environment, University of Oxford, Oxford OX1 3QY, UK.*
e-mail: marc.maciasfauria@ouce.ox.ac.uk

1. Baccini, A. *et al.* Science **358,** 230–234 (2017).
2. Delang, C. O. & Yuan, Z. *China's Grain for Green Program: A Review of the Largest Ecological Restoration and Rural Development Program in the World* (Springer, 2015).
3. Hua, F. *et al. Nature Commun.* **7,** 12717 (2016).
4. Tong, X. *et al. Nature Sustain.* **1,** 44–50 (2018).
5. Harkness, J. *China Q.* **156,** 911–934 (1998).

This article was published online on 22 January 2018.

In Retrospect

Eighty years of superfluidity

In 1938, two studies demonstrated that liquid helium-4 flows without friction or viscosity at temperatures close to absolute zero. The finding led to major advances in our understanding of low-temperature physics.

WILLIAM P. HALPERIN

In the early twentieth century, scientists discovered the non-intuitive phenomena of superconductivity and superfluidity, in which electrons and atoms, respectively, flow without resistance over great distances. Superfluidity was beautifully demonstrated 80 years ago in two papers published in *Nature* by Allen and Misener[1] and Kapitza[2]. The authors observed the flow of liquid helium-4 through extremely narrow channels and showed that the substance becomes a superfluid at very low temperatures. The studies presaged the firm understanding of the relationship between superfluidity and superconductivity that now exists, and which provides the foundation for investigating unconventional superconductors and superfluid phases.

Allen and Misener observed the flow of liquid helium-4 through long, thin tubes, and found that the fluid's viscosity became immeasurably low at temperatures below 2.17 kelvin. Kapitza obtained similar results by measuring the flow through a small gap between two glass disks (Fig. 1). With foresight, Kapitza noted a possible connection to superconductivity, for which a complete theory was eventually realized[3] in 1957 by Bardeen, Cooper and Schrieffer (BCS). Shortly after the two *Nature* papers were published, an explanation for the superfluidity of liquid helium-4 was offered: Bose–Einstein condensation[4], the process whereby many particles known as bosons 'condense' into a single quantum state.

In the quantum world, particles of the same type are indistinguishable, and there are only two classes of particle: fermions and bosons. However, an even number of interacting fermions can make a composite boson — for example, an atom of helium-4 is a composite boson that comprises six fermions (two protons, two neutrons and two electrons). At sufficiently low temperatures, helium-4 atoms undergo Bose–Einstein condensation and become a superfluid. Similarly, in the BCS theory of superconductivity, electrons that have a suitably attractive interaction can combine into charged composite bosons called Cooper pairs, which condense to form a superconductor.

In the wake of the Second World War, substantial quantities of the light isotope of helium, helium-3, became available through production of the heavy isotope of hydrogen (hydrogen-3 or tritium) for use in the hydrogen bomb. Because helium-3 contains an odd number of fermions (two protons, one neutron and two electrons), it is not a composite boson. It might therefore be considered that Bose–Einstein condensation could not take place and that helium-3 could never be a superfluid. However, the success of the BCS theory suggested another possibility: composite bosons comprising Cooper pairs of helium-3 atoms might condense into a superfluid, much like the electrons of a BCS superconductor.

The properties of this hypothetical superfluid were studied theoretically[5–7] in the 1960s. Research on the subject then exploded following the unexpected discovery[8] in 1972 of this superfluid at temperatures below 0.003 K. At first, the observations were interpreted as spontaneous nuclear magnetic ordering in solid helium-3, but shortly afterwards, they were correctly identified as the transition to a superfluid[9]. Nuclear magnetic ordering in solid helium-3 was discovered[10] two years later at a temperature of 0.001 K.

Cooper pairs have two types of angular momentum, characterized by the orbital quantum number (L) and the spin quantum number (S). Conventional BCS superconductors have $L = 0$ and $S = 0$, whereas superfluid helium-3 has $L = 1$ and $S = 1$. Nevertheless, the superfluid's properties can be understood using a modified version of the BCS theory[11]. The discovery of superfluid helium-3

50 Years Ago

There was an increase in the number of patients discharged from British hospitals in 1964, and a decrease in the average length of stay in hospital compared with 1962 and 1963. Men and boys stayed in hospital an average length of 18.3 days in 1964; women and girls … averaged just under two days less (16.7 days) … These are some of the findings in … the *Report on Hospital In-Patient Enquiry* for the year 1964 … The report contains detailed tables prepared from the 1964 ten per cent sample of discharges and deaths recorded … The tables are a mine of information … Injuries, poisonings and the like are all analysed in great detail according to whether they were caused by road traffic accidents, accidents in the home, or "other" mishaps.
From *Nature* 27 January 1968

100 Years Ago

It was stated officially … that the Admiralty had tested many methods of disguising mercantile shipping. One of these methods is to paint the ship with various quaint combinations of different colours. But this does not appear to have proved much of a success … Mr. Abbott H. Thayer … was one of the first to recognise that a high degree of invisibility is conferred on certain birds by the simple adaptation of being dark above and whitish below. He took two wooden decoy ducks, and placed them against a sandbank. One was coloured like the sand … the other was coloured on its upper parts darker than the surrounding sand, and graded below to pure white. At a short distance the first was still clearly visible, but the second was quite lost against its background … Some modification of this experiment has been tried on ships … but this device has not proved so successful as had been hoped.
From *Nature* 24 January 1918

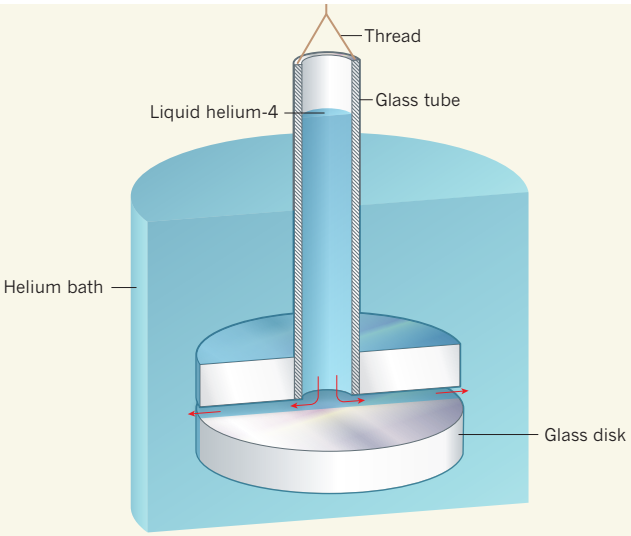

Figure 1 | Experimental evidence for superfluidity. In 1938, Allen and Misener[1] and Kapitza[2] showed that liquid helium-4 becomes a superfluid — a fluid with zero viscosity — at very low temperatures. Whereas Allen and Misener measured the flow of liquid helium-4 through long, thin tubes, Kapitza observed the flow (red arrows) from a glass tube to a helium bath, through a narrow gap between two glass disks. The separation between the disks was adjusted using a thread such that the level of the column of liquid in the glass tube was above the level of the helium bath. At temperatures above 2.17 kelvin, Kapitza found that the difference in height between these levels was maintained for several minutes. Conversely, at lower temperatures, the difference disappeared in seconds. Kapitza concluded that the viscosity of liquid helium-4 must be immeasurably low below 2.17 K. (Figure adapted from ref. 2.)

therefore marked the birth of unconventional superconductivity — and, more precisely, of superfluids that break certain fundamental symmetries of the normal (non-superfluid) state. The non-zero values of L and S in superfluid helium-3 correspond to broken rotational and time-reversal symmetries, which cause the substance to have a non-trivial topology.

In the absence of a magnetic field, superfluid helium-3 has two phases: A and B, with the B phase dominating the pressure–temperature phase diagram (a graph that plots the physical state of a material at various pressures and temperatures). The B phase can exist in many excited states, as a consequence of broken rotational symmetry associated with the total angular momentum of Cooper pairs[7,12,13]. The states of the B phase are classified by total angular momentum quantum numbers (J) of 0, 1 and 2. The $J = 2$ state comprises bosons that are analogous to the famous Higgs boson[14]. A remarkable finding is that the broken symmetry of the B phase, and its $J = 2$ state, enable the propagation of transverse sound waves[15,16] — a feature that was unheard of in liquids and was often assumed to be a property only of rigid solids.

Since the discovery of superfluid helium-3, many unconventional superconductors have been found. The best known are copper oxide compounds known as cuprates, which have the quantum numbers $L = 2$ and $S = 0$, and certain heavy fermion compounds[17]. However, only one superconducting compound, the uranium–platinum system UPt_3, has been discovered that has more than one superfluid phase, like helium-3. UPt_3 has $L = 3$ and $S = 1$, as predicted[18], and one of its phases breaks time-reversal symmetry in a similar way[19] to the A phase of helium-3.

In the past few years, helium-3 has been shown to exhibit new superfluid phases when confined to low-density materials called aerogels, small pores and narrow slabs[20]. Such phases are being investigated further. Eighty years after the discovery of superfluidity in liquid helium-4, the search is on for other scientifically interesting superfluids and superconducting materials. ■

William P. Halperin *is in the Department of Physics and Astronomy, Northwestern University, Evanston, Illinois 60208, USA.*
e-mail: w-halperin@northwestern.edu

1. Allen, J. F. & Misener, A. D. *Nature* **141,** 75 (1938).
2. Kapitza, P. *Nature* **141,** 74 (1938).
3. Bardeen, J., Cooper, L. N. & Schrieffer, J. R. *Phys. Rev.* **108,** 1175–1204 (1957).
4. London, F. *Nature* **141,** 643–644 (1938).
5. Anderson, P. W. & Morel, P. *Phys. Rev.* **123,** 1911–1934 (1961).
6. Balian, R. & Werthamer, N. R. *Phys. Rev.* **131,** 1553–1564 (1963).
7. Vdovin, Y. A. in *Application of Methods of Quantum Field Theory to Problems of Many Particles* (ed. Alekseyeva, A. I.) (GOS ATOM ISDAT, 1963).
8. Osheroff, D. D., Richardson, R. C. & Lee, D. M. *Phys. Rev. Lett.* **28,** 885–888 (1972).
9. Osheroff, D. D., Gully, W. J., Richardson, R. C. & Lee, D. M. *Phys. Rev. Lett.* **29,** 920–923 (1972).
10. Halperin, W. P., Archie, C. N., Rasmussen, F. B., Buhrman, R. A. & Richardson, R. C. *Phys. Rev. Lett.* **32,** 927–930 (1974).
11. Vollhardt, D. & Wölfle, P. *The Superfluid Phases of Helium 3* (Taylor & Francis, 1990).
12. Maki, K. *J. Low Temp. Phys.* **16,** 465–477 (1974).
13. Serene, J. W. III *Theory of Collisionless Sound in Superfluid Helium 3.* PhD thesis, Cornell Univ. (1974).
14. Volovik, G. E. & Zubkov, M. A. *J. Low Temp. Phys.* **175,** 486–497 (2014).
15. Moores, G. F. & Sauls, J. A. *J. Low Temp. Phys.* **91,** 13–37 (1993).
16. Lee, Y., Haard, T. M., Halperin, W. P. & Sauls, J. A. *Nature* **400,** 431–433 (1999).
17. Norman, M. R. in *Novel Superfluids* Vol. 2 (eds Bennemann, K.-H. & Ketterson, J. B.) Ch. 13 (Oxford Univ. Press, 2014).
18. Sauls, J. A. *Adv. Phys.* **43,** 113–141 (1994).
19. Schemm, E. R., Gannon, W. J., Wishne, C. M., Halperin, W. P. & Kapitulnik, A. *Science* **345,** 190–193 (2014).
20. Lee, Y. & Halperin, W. P. *J. Low Temp. Phys.* **189,** 1–14 (2017).

This article was published online on 15 January 2018.

BIOTECHNOLOGY

Kiss-and-tell way to track cell contacts

Transient cellular contacts are essential for the generation of an immune response, but these are difficult to measure *in vivo*. A labelling technique now offers a way to record such interactions between cells. SEE LETTER P.496

AARON P. ESSER-KAHN

Contact between two cells is a key step in the transfer of information during biological processes. However, monitoring dynamic cellular interactions *in vivo* poses many technical challenges. On page 496, Pasqual *et al.*[1] report the development of a technique that can track interactions between cells that contact each other through receptor–ligand binding.

A key step in the development of an immune response involves contact between an antigen-presenting cell (APC), such as a dendritic cell, and an immune cell called a T cell. On the APC surface, a receptor called the major histocompatibility complex (MHC) displays a protein fragment known as an antigen. If the

antigen is recognized by the receptor on the T cell, an immune response is triggered. Such cellular interaction is essential for the success of vaccination, cancer immunotherapy and the elimination of disease.

Pasqual and colleagues now describe a method that can quantify the interactions between APCs and T cells *in vivo*. The ability to count the frequency and number of interactions is fundamental to analysing many complex networks. For networks as diverse as Facebook, academic citations and molecular interactions in a biochemical pathway, such measurements are the main way of assessing the importance of an interaction. And yet for the immune system, which is key to good health, a simple tool to allow this has been lacking.

One current approach for mapping cellular interactions involves an enzyme-based labelling technique that measures static connections between neuronal cells grown in culture[2]. The authors describe an advance on this approach, using a form of enzyme-facilitated interaction mapping that is suited to the transient cellular interactions found in the immune system. Their method tracks the enzymatic transfer of a molecular label containing a small amino-acid tag, attached to an easily monitored molecule such as biotin. The molecular label can be transferred from one cell to another only if the cells are close enough together for an interaction to occur between a receptor and a ligand on the surfaces of the interacting cells. The molecular tag can then be detected by standard cell-analysis methods such as microscopy, or quantified *in vitro* using fluorescence analysis — tools already available to most biological researchers. The authors refer to this method of tracking a molecular 'kiss' between cells as LIPSTIC.

As a testing ground for their approach, Pasqual and colleagues choose a key interaction on the surface of immune cells that is highly dynamic and yet not physically involved in antigen presentation: the contact between a CD40L ligand, which is present on T cells, and its binding partner, the CD40 receptor, on APCs. Using mice, the authors engineered a fusion protein containing a sortase enzyme and CD40L, and generated a version of CD40 that contained glycine amino-acid residues at its amino terminus. The sortase was supplied with a labelling tag that became bound to the enzyme. In this system, when CD40 and CD40L interact, the sortase on the T cell attaches the tag to an N-terminal glycine residue on the APC's CD40 (Fig. 1).

LIPSTIC offers three major advances for the field. First, it allows the level of cell–cell interactions in the immune system to be quantified — the more APCs and T cells that interact, the higher the amount of cell labelling that is detected. Therefore, LIPSTIC provides a direct measure of a key step in the initiation of an adaptive immune response. It improves on current methods that measure this step indirectly, such as monitoring of the levels of inflammatory cytokine proteins or antibody production, which assess only the downstream effects of such interactions.

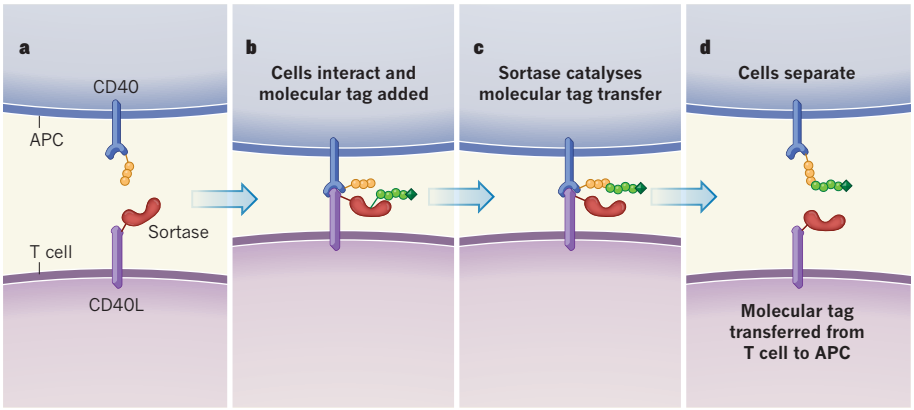

Figure 1 | Tracking cellular interactions. Pasqual *et al.*[1] describe a technique (termed LIPSTIC) that can monitor interactions between a T cell and an antigen-presenting cell (APC). **a**, Using mice for *in vivo* experiments, the authors generated T cells containing the CD40L ligand fused to the enzyme sortase, and APCs in which the CD40 receptor contains a few glycine amino-acid residues (yellow) at its amino terminus. **b**, When a CD40–CD40L interaction occurs between the cells, if a molecular tag consisting of a few amino acids (green circles) and the molecule biotin (green square) is added, the tag attaches to sortase. **c**, The enzyme then catalyses the transfer of the tag to a glycine on the amino terminus of CD40. **d**, When the cells separate, their interaction can be tracked by the presence of the transferred tag.

Second, LIPSTIC might offer the possibility of identifying the types of T cell with which APCs interact. Interactions between APCs and different T-cell types can determine both the nature and magnitude of an immune response. For example, the degree of activation of T cells that express the protein CD8 can provide a way of assessing the effectiveness of cancer immunotherapy[3]. Improved understanding of the interactions between T cells and APCs might thus allow the development of more-effective cancer immunotherapies and vaccines.

Third, and perhaps most impressively, the necessary tools and instrumentation for LIPSTIC analysis are readily accessible. This approach could therefore be rapidly implemented without the technology-transfer delays that often slow the adoption of a technical innovation.

To test LIPSTIC's usefulness for providing biological insights into immune-system function, the authors analysed the APC–T-cell interactions. Surprisingly, they found that these cells have two modes of interaction, although it had been thought that interaction occurs only when an antigen-bound MHC is presented to the T-cell receptor. The authors observed interaction between APCs and T cells that did not require an antigen-loaded MHC; the label was transferred onto cells that were not loaded with antigen. This previously unknown interaction would be difficult to observe without a method such as LIPSTIC. Why does it occur, and what purpose does it serve? The answers could have implications for efforts to improve immune responses.

Despite LIPSTIC's evident potential, many challenges remain that will determine the impact of this technique on the wider field of study of cell–cell interactions. How well will it work if adapted for use in systems other than those tested by Pasqual and colleagues? Another challenge will be to determine the level of nonspecific background labelling and of labelling errors inherent in the LIPSTIC approach. The ability to assess both the accuracy and precision of a labelling method is needed for all good quantitative tools.

One way in which the authors have already started to address the specificity of labelling is by using a sortase that has a low affinity for N-terminal glycines. However, the body is full of compounds that are similar to N-terminal glycines. Sortase, although specific for protein labelling *in vitro*, has not previously been used as a labelling tool in as reactive or demanding an environment as a whole organism. The potential for sortase to transfer a labelling tag to other biological entities at a low background level should be examined more fully. Nevertheless, the hitherto secret world of interactions between T cells and APCs can now be dissected and studied. LIPSTIC offers a way of quantifying contact, one of the most mysterious, but key, elements of a cellular network. ■

Aaron P. Esser-Kahn *is at the Institute for Molecular Engineering, University of Chicago, Chicago, Illinois 60615, USA.*
e-mail: aesserkahn@uchicago.edu

1. Pasqual, G. *et al. Nature* **553,** 496–500 (2018).
2. Liu, D. S., Loh, K. H., Lam, S. S., White, K. A. & Ting, A. Y. *PLoS ONE* **8,** e52823 (2013).
3. Mellman, I., Coukos, G. & Dranoff, G. *Nature* **480,** 480–489 (2011).

This article was published online on 17 January 2018.